Comparison Between Newtonian and Non-Newtonian Flow Driven By Internal Loads

O. Čadek, Y. Ricard, Z. Martinec, C. Matyska

Geophys. J. Int. (1993) **112,** 103–114

Comparison between Newtonian and non-Newtonian flow driven by internal loads

Ondřej Čadek,[1,2] Yanick Ricard,[1] Zdeněk Martinec[2] and Ctirad Matyska[2]

[1] *Département de Géologie, Ecole Normale Supérieure, 24 rue Lhomond, 75231 Paris, France*
[2] *Department of Geophysics, Charles University, V Holešovičkách 2, 180 00 Praha, Czechoslovakia*

Accepted 1992 July 13. Received 1992 July 13; in original form 1992 April 6

SUMMARY

The interpretation of long wavelength geoid and plate motions on the basis of dynamic Earth models has usually been done assuming linear viscous rheologies in the mantle. In this paper, we develop spherical 3-D models of mantle circulation using power-law creep rheologies with an exponent $n = 3$. We found that the stress-dependent rheologies only modify the amplitude of the topography supported by an internal load, by a small percentage with respect to the linear predictions. The geoid anomalies induced by internal loads can be affected by around 20 per cent. These changes are also occurring at degrees and orders different from those of the mass anomaly itself. As the geoid spectrum is strongly decreasing with degree, the dynamic topography induced at high degrees can be contaminated in a non-negligible way by the low degree loads. The main contamination occurs at a harmonic triple of that of the most important load. The flow structure is much more dependent on the creep law than are the dynamic topography and the geoid. In contrast to linear rheology, a power-law creep is able to sustain a toroidal velocity field. However, this toroidal component only carries a small percentage of the kinetic energy and thus the non-linear creep with $n = 3$ cannot by itself explain the observed quasi-equipartition of plate tectonic energy between toroidal and poloidal components.

Key words: geoid, non-linear rheology, plate motions.

1 INTRODUCTION

Since the 1980s, the global mantle dynamics has received renewed attention. Large scale asphericities have been revealed by seismic tomography (Dziewonski 1984; Woodhouse & Dziewonski 1984; Nataf, Nakanishi & Anderson 1986; Montagner & Tanimoto 1991). The nature of their relationships with the non-hydrostatic geoid is better understood (Ricard, Fleitout & Froidevaux 1984; Richards & Hager 1984) and a great effort is devoted to finding a consistent model of the mantle circulation of the Earth. Such a model has not only to satisfy the constraints imposed by seismic tomography but also to explain the gravitational field anomalies and the observed plate motion. This effort results in a number of models more or less consistent with observables (Hager *et al.* 1985; Forte & Peltier 1987; Ricard & Vigny 1989; Ricard & Bai Wuming 1991; Hager & Clayton 1989). The main conclusion of the above quoted papers is that a viscosity increase with depth is requested by the data. This viscosity increase is probably larger than a factor 10. However, different viscosity stratifications lead to an acceptable fit with the observations. Even the nature of the 670-km depth boundary cannot be constrained unambiguously by these models. If the mantle heterogeneities are of thermal origin, only models in which the flow can cross the upper–lower mantle interface explain the data. On the other hand, if one assumes that the strong upper mantle seismic heterogeneities are related to compositional changes and are not associated with lateral density heterogeneities, a two-layered mantle also satisfies the observations (Ricard, Vigny & Froidevaux 1989).

Besides their non-uniqueness, these models have a severe limitation: they are based on the assumption of a simple Newtonian rheology. This rheology is compatible with geophysical evidence but this cannot obscure the fact that the linear rheology was mainly chosen to simplify the analytical treatment of the problem. The question remains whether such a simplification is really justified. Microphysical analysis of creep mechanisms in polycrystalline silicates leads to the conclusion that processes in the mantle are most

probably governed by a non-linear constitutive law (Ranalli 1991). If this is the case, the geodynamical models derived under the assumption of Newtonian rheology may be seriously biased.

Several 2-D simulations of non-Newtonian convection have been performed (e.g. Parmentier, Turcotte & Torrance 1976; Cserepes 1982; Christensen 1984; Van Den Berg, Yuen & Van Keken 1992; Malevsky & Yuen 1992). Although the first 3-D computations of non-linear convection have already been reported (Christensen & Harder 1991), the sensitivity of 3-D solutions to the form of the constitutive law has not yet been satisfactorily described.

In the present paper, we compute and compare the flows induced by simple loads in a spherical shell for both Newtonian and non-Newtonian rheologies. The goal of this comparison is to emphasize the differences between linear and non-linear solutions and to estimate the limits of the classical linear modelling. The plan of our paper is as follows. In section 2, we formulate the forward problem of the mantle flow. In the Newtonian case, the problem is usually solved by means of a matrix propagator method. The non-linear problem requires a different approach. In this paper we employ the variational formalism discussed in section 3. The computations are performed for a rheologically homogeneous mantle shell with steady-state power-law creep. We only consider a stress exponent $n = 3$, a value which corresponds to the creep exponent found for olivine. To recognize easily the effects associated with a non-linear rheology, very simple driving forces, namely the buoyancy forces associated with simple harmonic loads, are prescribed.

The main results are discussed in section 4. The major attention is focused on the differences betweeen non-linear and Newtonian flow. We divide somewhat arbitrarily these differences into two effects. The first is the leakage of energy into modes different from the mode of the driving force. The second is the generation of a toroidal velocity field. Finally, we apply our understanding of non-linear behaviour to the interpretation of the geoid of the Earth and of the surface plate motions.

2 BASIC EQUATIONS

The flow in the mantle of the Earth induced by a body force $\mathbf{f}$ is governed by the equations of mass and momentum conservations,

$$\nabla \cdot \mathbf{v} = 0, \tag{1}$$

$$\nabla \cdot \boldsymbol{\tau} + \mathbf{f} = 0. \tag{2}$$

where $\mathbf{v}$ denotes the velocity and $\boldsymbol{\tau}$ is the stress tensor. Equation (1) assumes that the mantle is incompressible. We ignore the inertial forces in equation (2) since the mantle has a very large Prandtl number. We also neglect self-gravitation although we know that its effects can be significant at very long wavelengths. The mechanical behaviour of mantle material is characterized by the following rheological equation that relates the strain-rate tensor $\dot{\boldsymbol{\epsilon}}$ to the stress tensor $\boldsymbol{\tau}$:

$$\dot{\boldsymbol{\epsilon}} = \dot{\boldsymbol{\epsilon}}(\boldsymbol{\tau}). \tag{3}$$

The form of stress–strain relationship (3) depends on external physical conditions (temperature, pressure), microphysical state of the material (grain size), and on material parameters (lattice parameters, shear modulus...). Under a wide range of physical conditions, the mechanical behaviour of silicates and oxides can be described as follows (Ashby & Verrall 1977; Ranalli 1991):

$$\dot{\boldsymbol{\epsilon}} = A(\mathbf{D}:\mathbf{D})^{(n-1)/2}\mathbf{D}, \tag{4}$$

where $\mathbf{D}$ denotes the deviatoric part of stress tensor $\boldsymbol{\tau}$, $\mathbf{D}:\mathbf{D} = D_{ij}D_{ij}$ and n is a material constant. The other external and internal parameters are included in the factor A which is a function of spatial variables.

The Newtonian flow is characterized by $n = 1$. In this case, equation (4) reads

$$\dot{\boldsymbol{\epsilon}} = \frac{\mathbf{D}}{2\eta}, \tag{5}$$

where the Newtonian viscosity η, has been substituted for $1/2A$. The Newtonian viscosity in equation (5) as well as the parameter A in equation (4) are material parameters and thus, stress independent. Formally, equation (5) can also be used for non-Newtonian flow. In this case, however, an effective viscosity $\hat{\eta}$ is introduced. This viscosity is not a material parameter since it depends on stresses according to:

$$\hat{\eta} = \frac{1}{2A}(\mathbf{D}:\mathbf{D})^{(1-n)/2}. \tag{6}$$

The rheology of olivine and perovskite has recently been reviewed by Ranalli (1991). Extrapolation of laboratory experiments on olivine and their analysis by means of deformation maps lead to the conclusion that the upper mantle rheology could be predominantly non-Newtonian with an exponent close to 3. This conclusion is supported by observations of seismic anisotropy which cannot be explained satisfactorily by a linear creep mechanism (Karato 1988). In the lower mantle, the situation is more complex. Since direct laboratory investigations of perovskite are not yet possible, we can only rely on a few studies peformed on materials with analogue perovskite structure (Poirier *et al.* 1983; Beauchesne & Poirier 1989). Unfortunately, the results of these studies are still inconclusive as $n = 1$ as well as n close to 3.5 have been suggested. The form of the constitutive law governing the flow in the lower mantle still remains uncertain. In the present paper, we deal only with a non-linear flow characterized by a stress exponent $n = 3$. This value is consistent with the results of laboratory experiments on olivine and is also relevant in the lower mantle provided that the mechanical behaviour of perovskite is non-linear.

The solution of the Stokes problem defined by equations (1)–(3) requires the choice of appropriate boundary conditions. They can be formulated in terms of velocities,

$$\mathbf{v} = \mathbf{U} \text{ on } \Gamma, \tag{7}$$

of stresses,

$$\boldsymbol{\tau} \cdot \mathbf{v} = \mathbf{T} \text{ on } \Gamma, \tag{8}$$

or as a mixed boundary condition like the usual free-slip

condition,

$$\mathbf{v}\cdot\boldsymbol{\nu}=0, \quad \text{and} \quad \boldsymbol{\tau}\cdot\boldsymbol{\nu}-(\boldsymbol{\nu}\cdot\boldsymbol{\tau}\cdot\boldsymbol{\nu})\boldsymbol{\nu}=0 \text{ on } \Gamma. \tag{9}$$

In equations (7), (8) and (9), Γ represents the surface of the Earth and the core-mantle boundary, $\boldsymbol{\nu}$ is the unit outer normal to Γ, and $\mathbf{T}$ is the surface forces acting on Γ. In mantle flow modelling, the mixed free-slip boundary condition (9), corresponding to a zero radial velocity and a vanishing shear stress at the boundaries, has generally been used. The mantle flow driven by the observed plate motion has also been studied by means of models using equation (7) (e.g. Hager & O'Connell 1979). The goal of the present study is mainly to show the differences between Newtonian and non-Newtonian flows. That is why we will also prescribe the simple no-slip boundary condition

$$\mathbf{v}=0 \text{ on } \Gamma, \tag{10}$$

at both boundaries of the mantle. The boundary condition (10) is not very relatistic, at least at the core-mantle interface, but it leads to a very simple variational formulation of the Stokes problem (see section 3) and allows a demonstration of some non-linear effects.

Assuming a Newtonian mantle with a spherically symmetric viscosity structure the problem governed by equations (1), (2) and (5) can be solved by a standard spectral method. The body force $\mathbf{f}$ as well as the unknown functions $\boldsymbol{\tau}$ and $\mathbf{v}$ are expanded in terms of spherical harmonics and introduced into the appropriate equations. In this way, the partial differential equations, originally containing derivatives with respect to spatial coordinates, are decomposed according to degrees, and orders into sets of ordinary differential equations containing only functions of the radius. There are no couplings between unknowns of different spectral characteristics. For each degree and order, the equations can be solved analytically in some simple cases or numerically by a matrix propagator method (Gantmacher 1960). If the viscosity also depends on angular coordinates or if the rheology is non-linear the direct application of a matrix propagator technique is impossible. In that case, the ordinary differential equations for different degrees and orders are mutually coupled and all the non-linear equations must be solved simultaneously. The rules of mode coupling have been discussed elsewhere (Stewart 1992). When lateral viscosity variations are confined within a thin shell, solutions can be obtained for surface driven flows (Ricard, Froidevaux & Fleitout 1988) or for a real Stokes flow induced by internal loads (Ribe 1992).

Recently, some attention has been paid to a modification of the propagator technique for a more general case. By applying substitutions the problem can be reformulated so that the coupling terms are included in a formal body force. In this way, the equations are formally similar to those describing the flow in a shell with spherically symmetric viscosity. The solution of the problem is then found by applying an iterative procedure in which the solution found at the ith step is used to modify the source term in equations solved at the $(i+1)$th step. Using this semi-spectral iterative procedure, Colin & Fleitout (1991) deal with lateral viscosity variations in a Newtonian case with axi-symmetric geometry. Zhang & Christensen (1991) use a similar strategy to solve the same problem, but with a more general geometry.

3 VARIATIONAL FORMULATION OF THE STOKES PROBLEM

In general, physical processes can be formulated either in terms of differential equations or by means of integral relationships. The integral formulation is usually based on the energy balance or on applying variational principles to energy. The variational principles are very suitable for mathematical analysis as well as for numerical treatment of problems. From a physical point of view, they have the attractive feature of providing a deep insight into the physics of the problem. In this section, we present a variational formulation of the Stokes problem and we show it is a powerful tool for modelling the non-linear flow in the mantle.

Let us consider the following functional F of three independent variables, the deviatoric stresses $\mathbf{D}$, the pressure p and the velocity $\mathbf{v}$,

$$F(\mathbf{D},p,\mathbf{v})=\frac{1}{n+1}\int_M A(\mathbf{D}:\mathbf{D})^{(n+1)/2}\,dV + \int_M \mathbf{v}\cdot(\nabla\cdot\boldsymbol{\tau}+\mathbf{f})\,dV \tag{11}$$

where M is the mantle of the Earth. In equation (11), the stress tensor $\boldsymbol{\tau}$ is an implicit function of p and $\mathbf{D}$. The variation of F reads

$$\delta F(\mathbf{D},p,\mathbf{v})=\int_M A(\mathbf{D}:\mathbf{D})^{(n-1)/2}(\mathbf{D}:\delta\mathbf{D})\,\mathrm{dV} + \int_M \delta\mathbf{v}\cdot(\nabla\cdot\boldsymbol{\tau}+\mathbf{f})\,dV+\int_M \mathbf{v}\cdot(\nabla\cdot\delta\boldsymbol{\tau})\,dV. \tag{12}$$

By applying the Green theorem to the last term of equation (12) one can demonstrate that

$$\int_M \mathbf{v}\cdot(\nabla\cdot\delta\boldsymbol{\tau})\,dV=\int_\Gamma(\delta\boldsymbol{\tau}\cdot\mathbf{v})\cdot\boldsymbol{\nu}\,dS-\int_M\delta\boldsymbol{\tau}:\dot{\boldsymbol{\epsilon}}\,dV, \tag{13}$$

where $\boldsymbol{\nu}$ is the unit radial normal to the mantle boundary Γ. Combining equations (12) and (13) and employing the symmetry properties of both $\boldsymbol{\tau}$ and $\dot{\boldsymbol{\epsilon}}$, $\delta F(\boldsymbol{\tau},\mathbf{v})$ can be written:

$$\delta F(\mathbf{D},p,\mathbf{v})=\int_M(A(\mathbf{D}:\mathbf{D})^{(n-1)/2}\mathbf{D}-\dot{\boldsymbol{\epsilon}}):\delta\mathbf{D}\,dV + \int_M\delta p(\nabla\cdot\mathbf{v})\,dV+\int_M\delta\mathbf{v}\cdot(\nabla\cdot\boldsymbol{\tau}+\mathbf{f})\,dV + \int_\Gamma\mathbf{v}\cdot(\delta\boldsymbol{\tau}\cdot\boldsymbol{\nu})\,dS. \tag{14}$$

By setting δF to zero we can again derive the equations (1), (2), (4) and (10). This shows that equation $\delta F=0$ where F is given by equation (11), is equivalent to the differential formulation of the Stokes problem for the simple boundary condition (10).

What is the physical meaning of the above variational formulation? The first integral in (11) represents a dissipative energy and only includes the deviatoric stress tensor. The other integral incorporates the momentum equation: this term vanishes if $\boldsymbol{\tau}$ satisfies equation (2). The

solution of $\delta F = 0$ corresponds to the minimum of dissipative energy on the set of admissible stresses and velocities, defined by linear constraints (1), (2) and (10). If A is a constant, the dissipative energy is formally similar to the $L_{(n+1)}$-norm of $\mathbf{D}$. This indicates that a non-linear rheology tends to dampen the extremes of the deviatoric stress. This effect is more and more efficient as n increases. Fig. 1 helps to understand the shape of the functional F close to $\delta F = 0$ in a $\mathbf{v} - \mathbf{D}$ subspace. For a given $\mathbf{v}$, the functional has a minimum in $\mathbf{D}$. On the other hand, the functional is perfectly linear as a function of $\mathbf{v}$ for a constant $\mathbf{D}$ (see equation 11). In the valley of the functional F following the minimum of deviatoric stresses, the velocity reaches its maximum at the saddle point corresponding to the solution. From all the admissible stresses and velocities, the viscous system chooses the flow with the minimum dissipative energy and the maximum possible velocities. The real functional F is also pressure dependent. This arises from the last term of equation (11) that has an implicit dependence on $-\mathbf{v} \cdot p$ which in turn, shows that the functional has also a saddle point in the $\mathbf{v} - p$ subspace, but for a minimum in p.

There are several ways to find the saddle-point of functional F. The usual approach consists of a linearization of the problem by introducing an effective viscosity. This leads to an iterative procedure in which the value of effective viscosity at the $(i+1)$th step is computed from the velocities found in the ith step. This procedure, known as the method of secant modules (Nečas & Hlaváček 1981), is the variational analogue of the Picard method used for 2-D computations of non-linear time-dependent convection (Malevsky & Yuen 1991). Applications of the above method require the repeated solution of large sets of linear equations.

Another approach consists of applying gradient methods. Although these methods usually exhibit notoriously slow convergence near the solution, they do have some features which make them attractive. First, the gradient methods avoid the solution of large systems of equations, at the expense of a larger number of iterations. As the gradient (equation 14) can be expressed analytically after an expansion into harmonic functions, each iterative step is easy to perform. Second, since the inaccuracies in both rheology and body forces in the Earth's mantle are still very large, we do not need a method with an extremely high inner accuracy but rather a method which quickly gives the main features of the solution. The gradient methods satisfy this requirement. Moreover, we observe that the convergence generally has the form of dampened oscillations allowing the evaluation of the solution accuracy at each iteration. Third, the computation of a new solution for parameters close to the parameters used in a previous run is reached after only a few iterations.

In the present paper, we use a gradient method based on the Uzawa algorithm (Nečas & Hlaváček 1981). We start an iterative loop by computing the gradient of F with respect to the deviatoric stresses $\mathbf{D}$. We re-evaluate $\mathbf{D}$ by a line-search in the direction opposite to this gradient, while velocities and pressure are kept fixed. This brings the solution to the valley of the functional F depicted in Fig. 1. Then, the gradient with respect to velocity is computed and the solution is re-evaluated following this gradient, moving the solution on a line of constant $\mathbf{D}$ and p of Fig. 1. A new estimation of pressure is then deduced from a step in the direction opposite to the gradient of F with respect to p. After these three steps, in deviatoric stress, in velocity and in pressure, a new loop is performed until a satisfactory convergence is obtained.

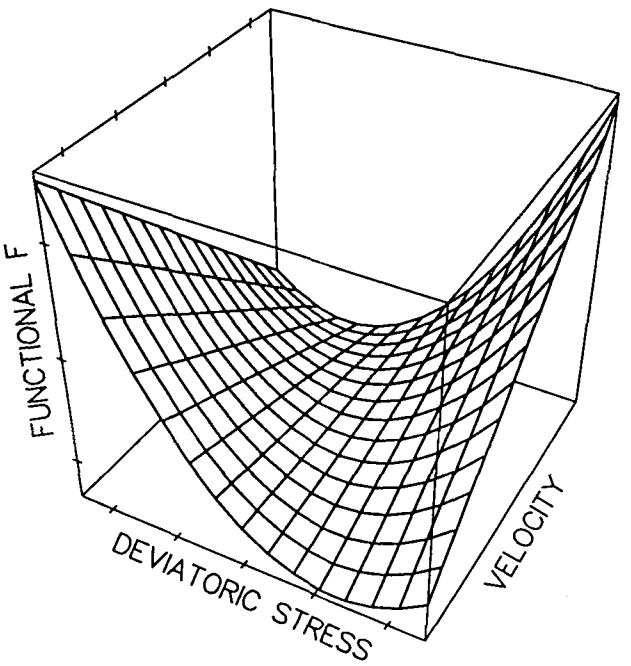

Figure 1. Schematic behaviour of the F functional around the solution in the $\mathbf{v} - \mathbf{D}$ subspace. The exact solution corresponds to the saddle point of this surface. The functional exhibits a minimum as a function of $\mathbf{D}$ but is linear in $\mathbf{v}$.

The tricky part of the algorithm is to choose the length of the steps in pressure and velocity, as no minima are present in these two directions. Physically, the amplitude of these steps can be chosen equal to 10 bars and 1 cm per yr, as an example. These steps are reduced if an oscillatory behaviour of the solution is found with amplitude larger than an *a priori* threshold. For geophysical purposes, an accuracy of 0.1 per cent on parameters is sufficient.

To express the functional F, we use a technique of spectral decomposition for the angular coordinates and a standard differential method in radius (Čadek, Martinec & Matyska 1992). The usual spectral decomposition consists in expressing the components of vectors and tensors in terms of scalar spherical harmonics and of their first order derivatives (e.g. Hager & O'Connell 1978). Since the application of this technique to tensor equations may be cumbersome we follow Jones (1985) and use generalized spherical harmonics. These harmonics are equivalent to, but formally different from the generalized spherical harmonics introduced in seismology by Phinney & Burridge (1973) and are also used in geodynamics (Ricard, Froidevaux & Fleitout 1988; Ribe 1992). Our formalism leads to a spectral decomposition which is consistent with the general formulation of the problem regardless of the value of the parameter n.

Fig. 2 illustrates an example of convergency of our algorithm. A simple harmonic load of degree 3 with

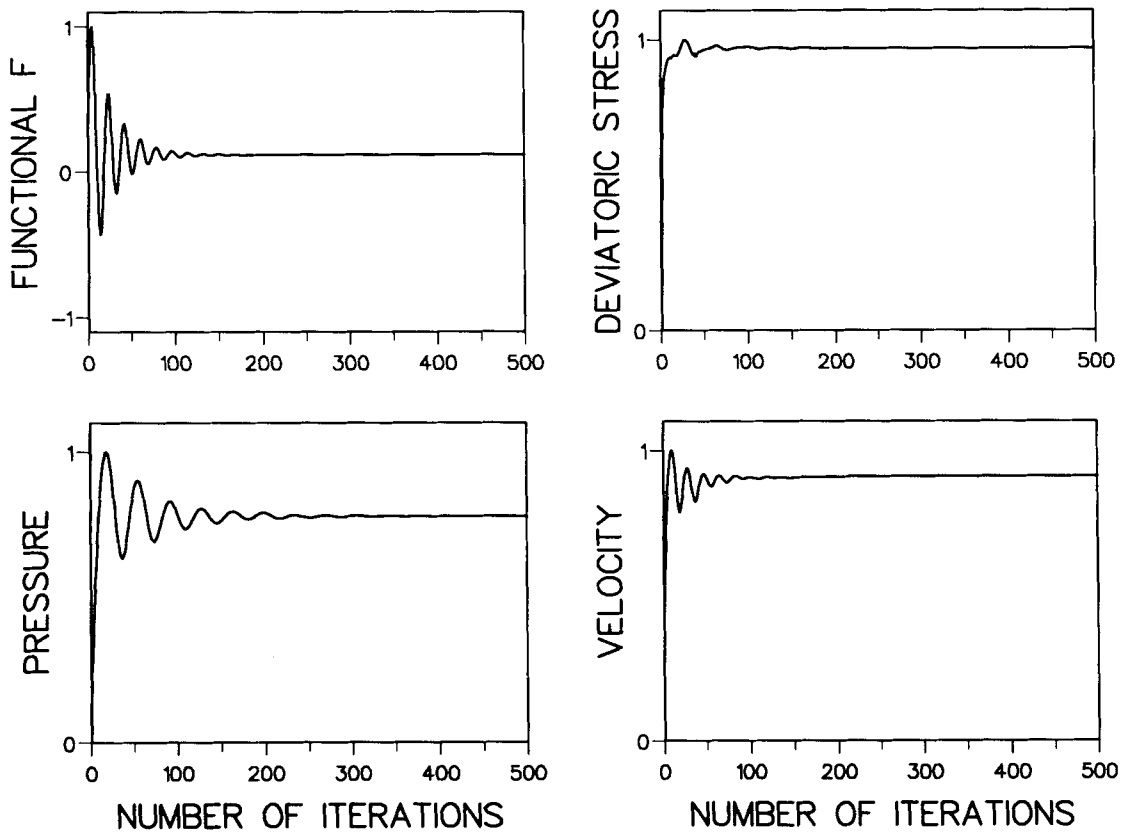

Figure 2. Behaviour of the functional F and of the three sets of variables during the search for the solution. The L_2-norm of the variables, normalized by the highest value obtained during the iteration is plotted. The convergency takes the form of dampened oscillations and the solution is reached after a few hundred iterations.

amplitude constant with depth is driving a flow in a non-Newtonian mantle with a power-law exponent $n = 3$. The harmonic expansions are truncated at degree 15. The mantle is divided into 20 layers of equal thickness. In this computation, the steps in pressure and velocity are kept constant. The top left panel depicts the behaviour of the functional F during the iterative procedure. The three other panels represent the L_2-norms of the three sets of variables. After 300 iterations, a stable solution is reached. The large number of iterations is related to the choice of the starting values for the unknowns to be identical to zero. When a more realistic initial solution, e.g. a solution obtained with a linear rheology, the number of iterations can be reduced by a factor 10.

The variational formulation (11) is only valid for no-slip boundary conditions given by equation (10) on both sides of the mantle. More realistic boundary conditions can be included in the following way

$$G(\mathbf{D}, p, \mathbf{v}) = F(\mathbf{D}, p, \mathbf{v}) - \int_{\Gamma_v} (\boldsymbol{\tau} \cdot \boldsymbol{\nu}) \cdot \mathbf{U}\, dS$$

$$- \int_{\Gamma_\tau} (\boldsymbol{\tau} \cdot \boldsymbol{\nu} - \mathbf{T}) \cdot \mathbf{v}\, dS - \int_{\Gamma_f} (\boldsymbol{\tau} \cdot \boldsymbol{\nu}) \cdot (\boldsymbol{\upsilon} - (\boldsymbol{\upsilon} \cdot \boldsymbol{\nu})\boldsymbol{\nu})\, dS, \quad (15)$$

where Γ_v, Γ_τ, and Γ_f are the different parts of the boundary where the conditions (7), (8) and (9) are prescribed, respectively. The reader can verify that $\delta G = 0$ corresponds to the requested solution.

4 COMPARISON BETWEEN NEWTONIAN AND NON-NEWTONIAN FLOW

The linear processes are characterized by the principle of superposition: if $S_1(\mathbf{f}_1)$ and $S_2(\mathbf{f}_2)$ are solutions corresponding respectively to the body forces $\mathbf{f}_1$ and $\mathbf{f}_2$, then the flow induced by the force $\mathbf{f}_1 + \mathbf{f}_2$ is simply the sum of solutions S_1 and S_2. For the non-Newtonian rheology the principle of superposition is not valid any more. Another elementary property of non-linear flow follows directly from the variational equations (15) and (16): for a given distribution of body force $\mathbf{f}$ and imposed no-slip or free-slip boundary conditions, the dependence of stress on the magnitude of this body force is linear regardless of the value of the creep exponent n. In constrast, the velocity is proportional to the nth power of $\mathbf{f}$. In other words, if $\boldsymbol{\tau}$ and $\mathbf{v}$ solve the Stokes problem for a given body force $\mathbf{f}$, the solutions for the body force $\alpha \cdot \mathbf{f}$, where α is a real number, are $\alpha\boldsymbol{\tau}$ and $\alpha^n\mathbf{v}$. While an increase of the body force $\mathbf{f}$ by a factor 2 generates stresses two times higher, it generates a velocity increase by a factor 8 if $n = 3$.

The method described in the previous section can be used for an arbitrary rheological function A and for various values of the stress exponent n. Here, we consider only a

simplified physical model of the mantle where the parameter A is constant with depth. In such a rheologically homogeneous mantle we compute the non-linear flow ($n = 3$) induced by a given distribution of the buoyancy force and we compare it with the Newtonian flow driven by the same body force distribution.

Leakage of the dissipative energy into different modes

In a Newtonian mantle with a spherically symmetric viscosity structure, a body force of a given degree and order can only drive a motion which has the same spectral characteristics. In contrast, a non-linearity of the stress–strain relationships leads to a partial redistribution of the dissipative energy among other modes. This means that a pure harmonic body force can drive a motion characterized by a large number of spectral terms.

This feature of the non-linear flow is illustrated in Fig. 3 where the spectral response to a simple load ($l = m = 1$) is shown. The magnitude of the load is constant with depth and two different boundary conditions are used. The spectral amplitude of a given variable of degree l is the L_2-norm of its distribution throughout the mantle. The black circles correspond to a no-slip boundary condition (10) at both sides of the mantle. The results obtained for a free-slip condition (9) are depicted by a square. For pressure and deviatoric stresses, the amplitudes have been normalized by the values obtained for a linear case with free-slip boundary conditions. The parameter A scaling the amplitude of velocity is chosen to give a spectral component of degree $l = 1$ equal to 1 when free-slip conditions are applied. The term of degree 1 remains dominant but other non-zero modes appear. These modes are confined to odd degrees by symmetry. The leakage is especially visible in the spectra of velocity and deviatoric stress, while the pressure spectrum is more weakly disturbed. The components of degree 3 of the first two fields in the no-slip case are larger than 10 per cent of the amplitude of degree 1, but the pressure of degree 3 is less than 4 per cent of that of degree 1. The no-slip boundary condition strongly dampens the velocity. It also concentrates the deviatoric stresses on both sides of the mantle and thus enhances the non-linear effects. This explains why the ratio between the fundamental velocity mode ($l = 1$) and the first excited harmonic ($l = 3$) is somewhat smaller in this case then when a free-slip condition is applied.

Although the higher modes in the spectrum of velocity are smaller by 1 or 2 orders of magnitude than the term of degree 1, they are able to change considerably the global flow pattern. A comparison between the Newtonian and non-Newtonian style of circulation is given in Fig. 4 (a and b), where the flows at 1000 km depth are depicted. To emphasize the differences between the two patterns, we apply the no-slip conditions that lead to a larger relative amplitude of high modes than the free-slip conditions. The Newtonian viscosity and the parameter A in the non-linear case have been chosen so that the two flows have the same maximum velocity. The Newtonian flow correlates with the lateral distribution of the density anomaly and the maxima of vertical motion coincide with the maxima of the buoyancy force. The non-Newtonian rheology leads to a strikingly different pattern as the maximum of vertical motion forms a ring around the centre of the load. Such an effect has not been observed using free-slip boundary conditions.

The fact that, between the up- and down-welling zones, the vertical velocity changes more abruptly in the non-linear case than in the Newtonian is easy to understand. The effective viscosity distribution shows a significant increase close to the centre of the load where the deviatoric stresses are minimum (see equation 6). Two high viscosity plugs tend to slow down the flow and to push it toward regions where the body force is somewhat smaller but where the viscosity is low enough to allow the material circulation (Froidevaux 1973).

The simple example discussed above illustrates stumbling-blocks associated with the interpretation of non-linear flows

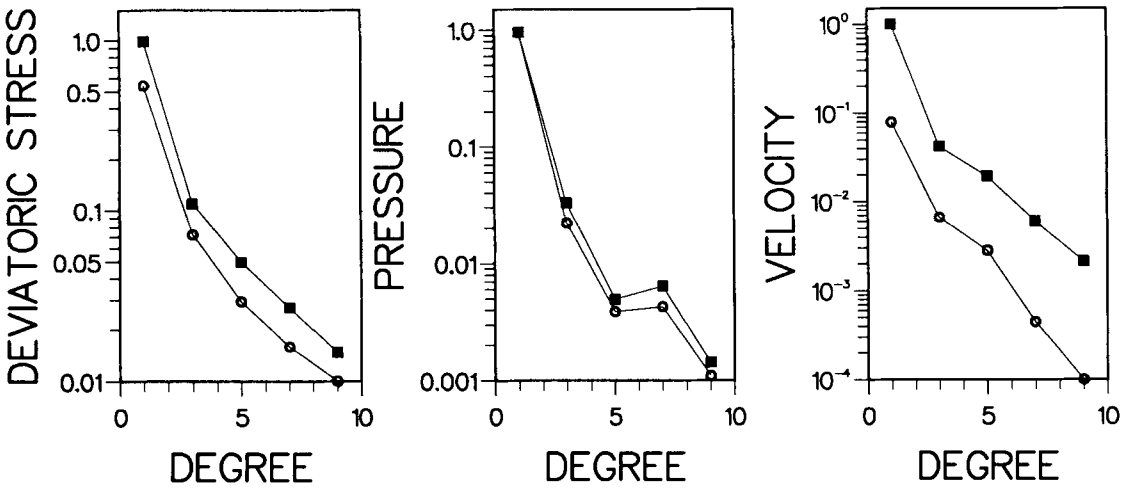

Figure 3. L_2-norm spectra of deviatoric stresses, pressure and velocity. The load exciting the flow is a pure harmonic function of degree 1 constant with depth. The results for free-slip and no-slip boundary conditions are depicted with squares and circles, respectively. The spectra of pressure and deviatoric stress are normalized by their values obtained with a free-slip model computed using a linear rheology. The amplitude of the degree 1 velocity is scaled to 1 for the free-slip model. The non-linearity of the constitutive relationship induces terms of degrees larger than 1. Their amplitudes are a small percentage of the amplitude of degree 1.

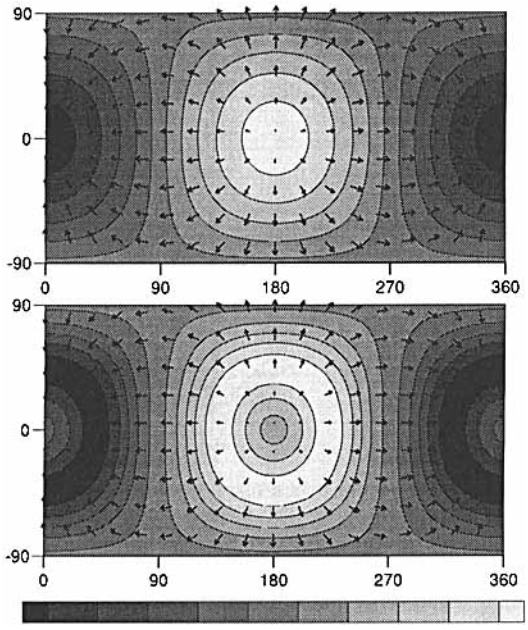

Figure 4. Flow at the depth of 1000 km, induced by a pure harmonic load of degree 1. The amplitude of the load is constant with depth. No-slip boundary conditions have been applied on both sides of the mantle. On top (a), the mantle rheology is linear. The bottom (b) has been computed for a rheology with power-law exponent $n = 3$. The vertical flow is shown by means of a shadow pattern. In the non-Newtonian case the width of the vertical currents widens.

by means of an effective Newtonian model. To explain the velocity field shown in Fig. 4b, one would have either to admit a more complex density structure containing loads of degree 3, 5, 7..., or to introduce lateral variations of viscosity. Both interpretations are misleading: the former gives a wrong density structure, while the latter leads to the conclusion that regions of minimum densities have higher viscosities, even though they could be expected to be associated with hotter and less viscous material.

The pressure is much less sensitive to the change of the power law exponent n than the velocity. The same is valid for the dynamic topography formed by the non-linear flow at the boundaries of the mantle. Although its shape, proportional to the vertical stress, is influenced by the velocity gradient which may strongly depend on the rheology, the topography at low degrees mainly reflects the pressure variations. The geoid undulations associated with internal loads are crucially dependent on the induced topography. In fact, the potential perturbation associated with only the internal masses is of the same amplitude as the potential perturbation associated with the topography but of the opposite sign (Ricard *et al.* 1984; Richards & Hager 1984). As the geoid modelling in conjunction with seismic tomography has been used to infer the mantle viscosity profile, it is important to verify if the conclusions drawn within the framework of linear models hold for non-linear models.

In the linear case, the relationships between internal loads and surface observables (topography, geoid, surface divergence field) are often expressed by means of Green functions. Such kernels are only meaningful when the modes are completely decoupled, which is not the case using non-linear rheologies where the responses are also a function of the order m of the source. Nevertheless, to quantify the possible drawbacks in the interpretation of the long-wavelength geoid, we compute the response functions associated with zonal harmonics and compare them to the usual Green function. A response function is simply the response of the non-linear mantle to a load expressed as the product of a pure spherical harmonic by a delta function in radius. By symmetry, zonal harmonics distribute their energy only to other zonal harmonics.

Fig. 5 depicts the divergence, topography and geoid induced by a load of degree 2 and order 0 located at a given depth in a mantle with power law rheology. Dashed lines correspond to the usual Green functions computed for a uniform Newtonian mantle with viscosity η_0. We chose η_0 and A so that the maximum of divergence for degree 2 is 1. The distribution of energy on the other modes is very important for the divergence field. The major contamination arises at degree 6 (26 per cent of degree 2 amplitude) then, at degree 4. The topographies are normalized with respect to the surface value which in both cases corresponds to perfect isostasy. The amplitude of the degree 2 non-linear response is basically identical to the linear Green function. The contamination on other degrees is almost negligible. The geoid is more sensitive than topography to the rheology as it is related to the difference between two approximately opposite contributions, the potential of the load and the potential of the deflected interfaces. On the right panel the geoid contribution of degree 2 and the Green function are normalized by $4\pi Ga/(2l+1)$ where G is the gravitation constant and a the radius of the Earth. While the two curves are somewhat similar, differences of more than 30 per cent exist between them at certain depths in the lower mantle. The contamination on higher modes seems rather weak, and like for the divergence affects degree 6 more than degree 4. However, taking into account the fact that the observed geoid spectrum strongly decreases with l and that its degree 2 has an amplitude more than 3 times larger than that of degree 4, and more than 6 times larger than that of degree 6, one can see that the geoid of degree 4 and 6 may be strongly contaminated by non-linear effects related to loads of degree 2.

Modelling of the long wavelength geoid in the framework of Newtonian models has suggested an increase in the mantle viscosity at the upper–lower mantle interface. It is not so easy to translate such a viscosity increase in terms of non-Newtonian rheology as we are able to control the parameter A, but not the effective viscosity. Fig. 6 depicts the same observables as Fig. 5, but for a non-Newtonian mantle where A is increasing by a factor 1000 at 670 km depth. The shapes of the three response functions are close to the Green function obtained for linear models with a viscosity increase with depth. The surface divergence is little affected by loads stuck in the highly viscous lower mantle. The loads are efficiently supported by the stiff lower mantle and the induced topography at the surface of the Earth is strongly decreasing with the depth of the load. As a consequence of this decrease in amplitude of topography, the geoid changes sign. An interesting point is that the

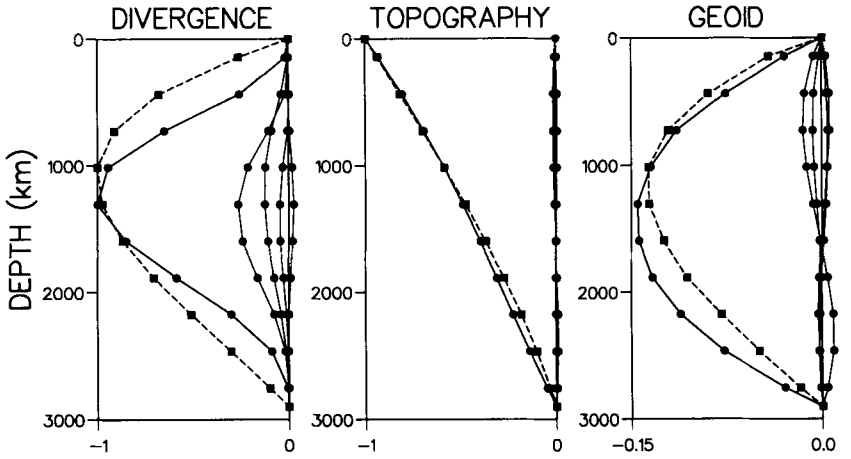

Figure 5. Surface divergence, topography and geoid induced by a unit load of degree 2 and order 0 as a function of the depth of load. The dashed line corresponds to the Green functions obtained for a linear rheology with uniform viscosity. The full lines depict the amplitudes of components of degrees 2, 4, 6, 8. . . , excited in a mantle with power law creep. The divergence curves have been normalized with respect to the maximum values obtained at degree 2. The topographies are equal to −1 at the surface, a value which corresponds to a perfect isostatic compensation. The geoid curves are in units of $4\pi Ga/(2l+1)$ where G is the gravitation constant and a the Earth's radius.

response functions for an increase in A by a thousand roughly correspond to the Green functions obtained for a viscosity increase of only about 10–50 (e.g. Hager & Clayton 1989). The mapping of an increase in A into an increase in Newtonian viscosity is obviously non-linear. The leakage between modes is lower in the stratified case (Fig. 6) than in the uniform case (Fig. 5).

In Newtonian models with lateral viscosity variations where density and viscosity variations are related, the most severe contamination occurs at the doubled harmonic of the dominant heterogeneity (e.g. Richards & Hager 1989). We can qualitatively understand why we instead obtain most of the contamination at the triple harmonic. The couplings occur in the constitutive equation (3). For lateral viscosity variations in phase with density, both deviatoric stresses and inverse of viscosity are essentially of the same degree l and therefore the strain tensor related to their product is mostly of degree $2l$. In the non-linear case with a power law exponent $n = 3$, the inverse effective viscosity corresponding to a load of degree l is proportional to the square of stresses, and has a dominant degree $2l$. Therefore, the strain tensor is mostly affected at degree $3l$.

Generation of the toroidal flow

Any vector field $\mathbf{v}$ satisfying the equation of incompressibility (1) can be expressed as the sum of a toroidal and a

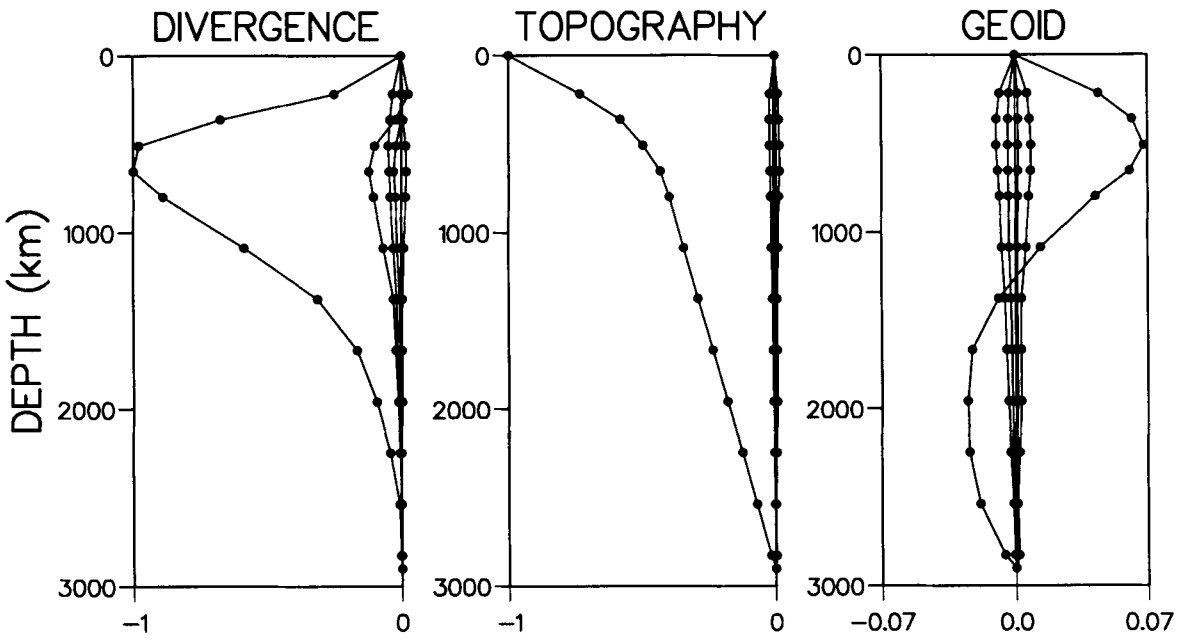

Figure 6. Same as Fig. 5, but for an increase of the parameter A by a factor 1000 at a depth of 670 km.

poloidal velocity field

$$\mathbf{v} = \mathbf{v}_t + \mathbf{v}_p. \tag{16}$$

The toroidal flow $\mathbf{v}_t$ has no radial component and its horizontal divergence is equal to zero

$$\nabla_H \cdot \mathbf{v}_t = 0. \tag{17}$$

The poloidal component $\mathbf{v}_p$ carries the vertical flow, it has a zero radial vorticity,

$$\mathbf{v} \cdot (\nabla \times \mathbf{v}_p) = 0. \tag{18}$$

In a convective system, the decomposition (16) has a clear physical meaning. The mantle flow results from the convective cooling of the Earth but only the poloidal motion transports heat from the deep layers to the surface. The toroidal motion, having a zero radial component, does not take part in the heat transfer directly. It mainly represents resistive processes associated with the existence of lithospheric plates. It also takes part in the horizontal redistribution of mantle material and participates in the heat transfer in this way.

One can easily demonstrate from the Navier–Stokes equation that buoyancy forces cannot drive any toroidal motion in a mantle with a Newtonian viscosity varying only with depth. In a non-Newtonian mantle, however, the toroidal flow quite naturally arises from the non-linear interaction of poloidal terms. An interesting point is that no toroidal motion seems to be excited by a pure harmonic load in a non-linear mantle.

An example of generation of toroidal flow is given in Fig. 7, where the surface motion driven by loads of degree 1 order 1 and degree 2 order 0 is shown. The two loads are constant with depth and have the same amplitude. On top of the mantle viscosity is Newtonian whereas the middle panel is for a non-Newtonian flow with $n = 3$. The amplitudes of the two velocity patterns have been chosen so that they give the same maximum amplitude. The difference between the two maps is visible around longitude 0° or 360°, where the non-Newtonian flow is basically stagnant. The bottom panel shows the toroidal component included in the non-Newtonian velocity pattern. Here, the lengths of the arrows have been multiplied by ten with respect to those of the top and middle panels. In this case the toroidal kinetic energy is only 1.5 per cent of the total energy. However, the toroidal velocity reaches an amplitude close to 10 per cent of the poloidal velocity.

Fig. 8 shows the poloidal and toroidal spectra of the surface velocity. The loads are of degrees 1 and 2, and these degrees are dominant in the poloidal velocity spectrum. All the other degrees of the poloidal field and those of the toroidal are induced by mode coupling. The amplitude of toroidal velocity at degree 2 reaches 20 per cent of the poloidal velocity at the same degree. For some degrees, namely 4, 7 and 10, the ratios between toroidal and poloidal velocity are as high as 50 per cent.

There is no direct evidence of the amount of toroidal energy inside the real mantle but some indications can be retrieved by analysing the observed surface velocities. The present time plate motion is characterized by a quasi-equipartition of kinetic energy between poloidal and toroidal modes (Hager & O'Connell 1979). The main part of

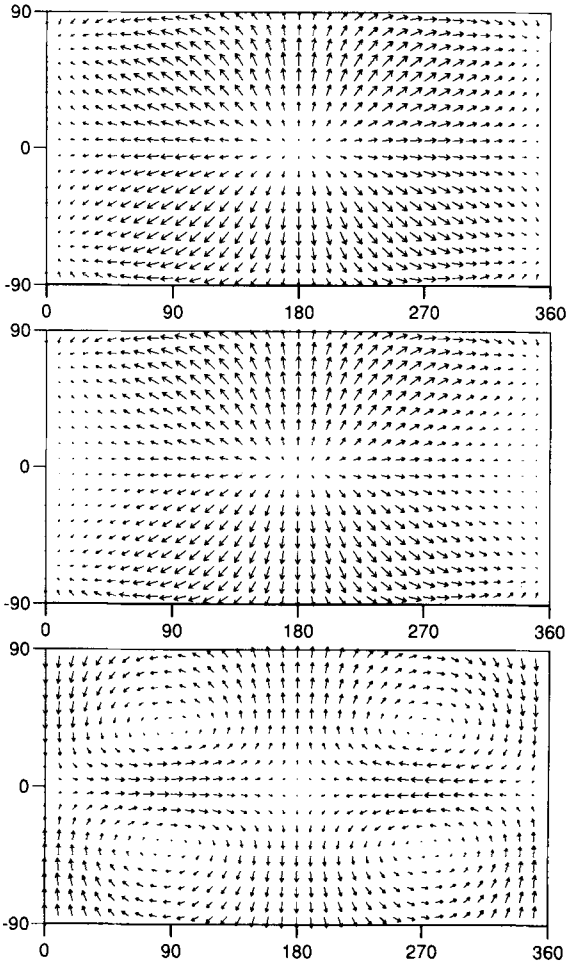

Figure 7. Surface motions induced by loads of degrees 1 and 2 in a Newtonian mantle (top panel) and in a non-Newtonian mantle (middle panel). The bottom map depicts the toroidal component of the non-Newtonian flow with an increase in the lengths of arrows by a factor of 10.

toroidal energy, however, is a consequence of the geometry of plates which are driven by poloidal forces (Ricard & Vigny 1989, O'Connell & Hager 1991; Čadek & Ricard 1992). Nevertheless, a small part of plate energy (about 5 per cent) responsible for the spin of plates is probably a consequence of toroidal flow in the sublithospheric mantle (Olson & Bercovici 1991). The computations carried out for simple combinations of harmonic loads lead to the conclusion that the total amount of toroidal energy in a homogeneous mantle governed by power-law creep with $n = 3$ is the same amount. Such a small percentage of toroidal flow is also found in numerical calculations of 3-D thermal convection with variable viscosity (Christensen & Harder 1991).

Implications for the real Earth

The knowledge of the real mantle rheology and of mantle mass anomalies is too uncertain to develop a realistic model of mantle circulation including a possible non-linearity in the constitutive relationship. However, we present a computa-

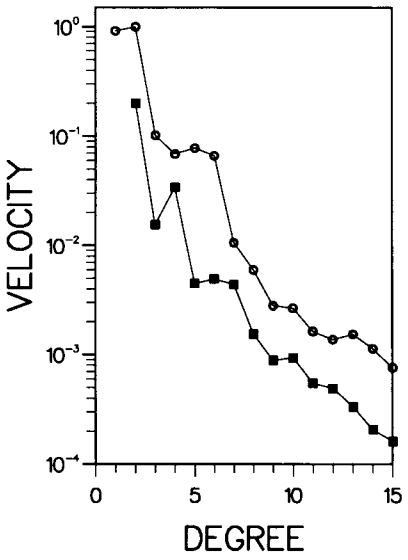

Figure 8. Spectra of poloidal (circles) and toroidal (squares) velocity components of the flow pattern given in Fig. 7 (middle). The large poloidal components of degree 1 and 2 correspond to the loads. All the other terms are induced by mode coupling.

tion that allows a quantitative evaluation of the possible drawbacks in geoid and plate motion simulations induced by a neglect of non-linear effects of the mantle rheology.

The geoid undulations of the Earth are probably induced at degrees 2 and 3 by lower mantle mass anomalies, whereas the components of higher degrees are strongly related to the presence of slabs in the upper mantle (e.g. Hager & Clayton 1989). We use these results to build a very simple model of mantle heterogeneities where the anomalies of degrees 2 and 3 are only located at a depth of 2000 km and where those of degrees 4, 5 and 6 are located in the upper mantle at a depth of 400 km. Our distribution of density anomalies convolved with the Green functions computed for a homogeneous Newtonian mantle reproduces exactly the observed geoid. We know that the homogeneous Newtonian mantle does not correspond to the real situation in the Earth where a large viscosity increase with depth is likely to occur. We choose such a simple rheological model to avoid the difficult mapping of linear viscosity profiles into profiles of A. Using our model of density distribution, we compute the induced flow and the resulting geoid for both linear and non-linear rheologies. Our model of mass distribution induces an unrealistic velocity pattern at the surface as it does not include the masses associated with slabs and ridges that drive the plate motion. However, we think that the comparison between the linear and the non-linear surface flows is indicative of the effects that might occur for the real Earth.

Fig. 9 shows the geoids computed with a uniform linear rheology (top) and with a non-linear rheology (middle). By construction the top map is the observed geoid filtered for degrees larger than 6. The middle map includes all the degrees up to $l = 15$. The bottom map depicts the difference between the middle and top maps. The geoid computed with a non-linear rheology has a larger amplitude than the real geoid. This related to the larger response functions already

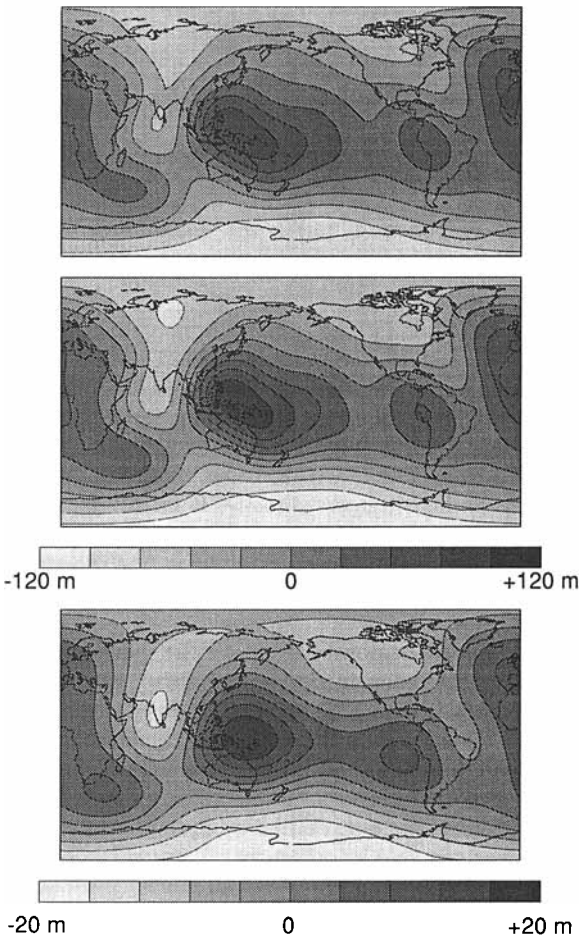

Figure 9. Synthetic non-hydrostatic geoids in meters obtained with a linear rheology (top) and a non-linear rheology (middle). The difference between them is plotted in the bottom map with a different scale. We choose the mantle density so that the top map exactly fits the real geoid up to degree 6. A change in the rheology modifies the amplitude of the geoid more than its shape.

seen in Fig. 5. The bottom map has an amplitude reaching 20 per cent of that of the real geoid and is highly correlated with it. This suggests that the interpretation of the geoid by means of a linear rheology might lead to an overestimation of the lower mantle density heterogeneities by some 20 per cent, if the mantle is really non-linear. The changes in geoid heights are related to a change of the induced topography. As was already clear from Fig. 5, this change of topography is very small.

Fig. 10 depicts the surface divergences induced at the surface of a Newtonian mantle (top), a non-Newtonian mantle (middle) and the difference between the two (bottom) in the same way as Fig. 9. Our oversimplified model of mantle density induces upwellings beneath the geoid highs which are obviously not observed. The viscosity and the parameter A are chosen so that the top and middle maps have the same maximum. The differences between the results are more striking than in Fig. 9. The non-linearity increases the flow where the Newtonian velocities are already large and dampen the flow elsewhere. This is why, in the middle map, the flow is rather stagnant in the east Pacific and the Atlantic with respect to the west Pacific

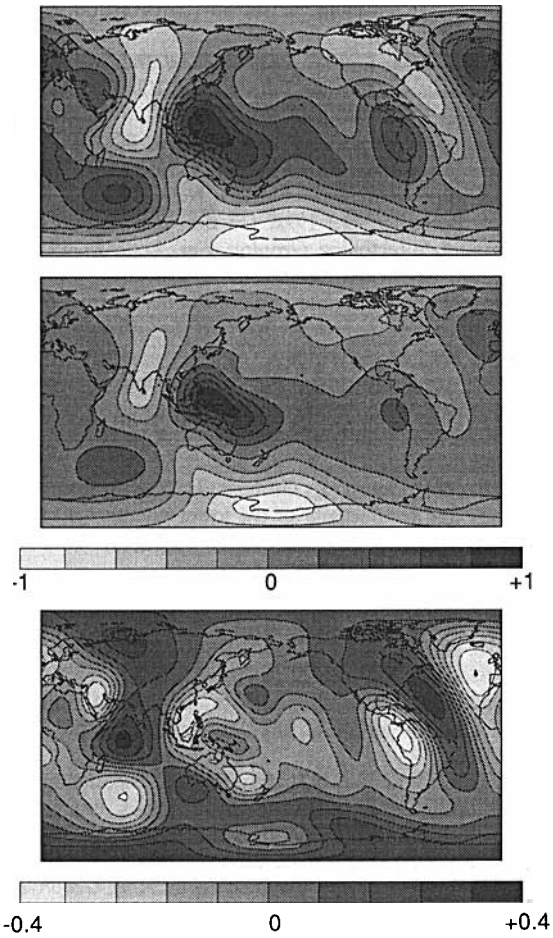

Figure 10. Synthetic surface divergence obtained with a linear rheology (top) and a non-linear rheology (middle). The difference between them is plotted in the bottom map with a different scale. The top and middle maps have been normalized by their respective maxima. A change in the rheology modifies the shape of the predicted divergence.

upwelling. For the geoid, the difference between the two rheologies is mainly a weak change in the amplitude. For the velocities, the pattern itself is rather different, leading to a maximum change in magnitude close to 40 per cent of the signal.

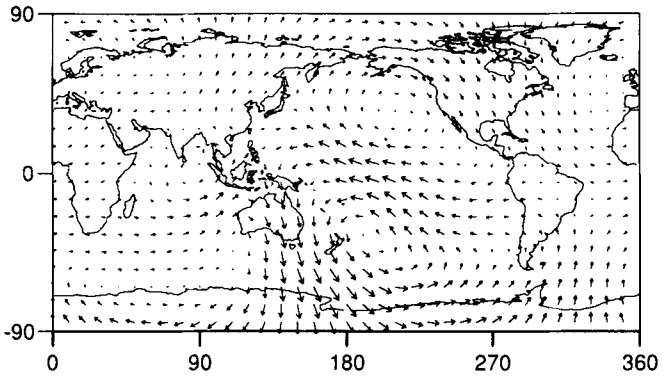

Figure 11. Toroidal velocity field induced at the surface of our model. The maximum velocity reaches 15 per cent of the maximum poloidal velocity associated with the divergence plotted in Fig. 10 (middle).

The use of a non-linear rheology also generates a toroidal motion. The maximum toroidal velocity is around 15 per cent of the poloidal one (Fig. 11). As for the surface divergence, the toroidal velocities are mainly excited where the flow predicted with a linear viscosity is already vigorous, i.e. around the west Pacific margin; it is stagnant elsewhere.

5 CONCLUSIONS

This paper has shown the efficiency of variational formulations for mantle dynamics. With a simple gradient method we reach the solutions of non-linear 3-D problems even when large jumps in mechanical properties are present. The number of iterations needed to reach the convergence is quite large but the computation can be performed on a simple work-station. Our method can also be easily used for intrinsic viscosity variations within the mantle.

An important result of the present study is that Newtonian and non-Newtonian flow can be very different while the distribution of pressure does not significantly change. The non-linearities contaminate modes with degrees different from those of the load. When there is dominant degree in the load, the main contamination occurs at a degree triple from the main load. This result differs from the observation of Newtonian flows with lateral viscosity variations in phase with loads where the doubled harmonics are mostly contaminated.

The steady-state surface deformations that we compute are found to be not very sensitive to the form of the constitutive equation. Our study does not address the problem of transient deformation such as post-glacial rebound. The time-varying topographies involved in transient problems are directly related to the computation of vertical velocities and should be much more sensitive to the rheological law (e.g. Wu 1992; Gasperini, Yuen & Sabadini 1992).

The geoid anomalies are affected by the pressure field inducing dynamic topographies at the surface of the Earth and at the core-mantle boundary. Although more sensitive than the topographies, the geoid prediction is still robust with respect to the constitutive law. A neglect of non-linear rheology affects mainly the estimation of the sources amplitude. This is a small effect in comparison with the present uncertainties in the mantle heterogeneities and in the mechanical stratification of the mantle.

The prediction of plate motions from internal loads may be strongly affected by non-linearities. The velocities computed with non-linear rheologies are enhanced where linear models already predict large velocities. A toroidal field is induced by the coupling of modes. However, the related kinetic energy is only a small percentage of the total energy and thus, a power-law creep with $n = 3$ cannot by itself explain the observed equipartition between toroidal and poloidal energy.

ACKNOWLEDGMENTS

This work was partly supported by the INSU-DBT (Dynamique et Bilan de la Terre) program (Global Dynamics, contribution 477).

REFERENCES

Ashby, M. F. & Verrall, R. A., 1977. Micromechanisms of flow and fracture, and their relevance to the rheology of the upper mantle, *Phil. Trans. R. Soc. Lond. A*, **288,** 59–95.

Beauchesne, S. & Poirier, J. P., 1989. Creep of barium titanate perovskite: a contribution to a systematic approach to the viscosity of the lower mantle, *Phys. Earth planet. Interiors*, **55,** 187–199.

Čadek, O., Martinec, Z. & Matyska, C., 1992. Spectral variational approach to the non-Newtonian Stokes problem in a spherical shell, *Comput. Phys. Communs*, in press.

Čadek, O. & Ricard, Y., 1992. Toroidal/poloidal energy partitioning and global lithospheric rotation, *Earth planet. Sci. Lett.*, **109,** 621–632.

Christensen, U., 1984. Convection with pressure- and temperature-dependent non-Newtonian rheology, *Geophys. J. R. astr. Soc.*, **77,** 343–384.

Christensen, U. & Harder, H., 1991. 3-D convection with variable viscosity, *Geophys. J. Int.*, **104,** 213–226.

Colin, P. & Fleitout, L., 1991. Interaction of deep mantle heterogeneities with the lithosphere, in *Abstracts of XX General Assembly IUGG*, Vienna.

Cserepes, L., 1982. Numerical studies of non-Newtonian mantle convection, *Phys. Earth planet. Interiors*, **30,** 49–61.

Dziewonski, A. M., 1984. Mapping the lower mantle: determination of lateral heterogeneity in *P* velocity up to degree and order 6, *J. geophys. Res*, **89,** 5929–5952.

Forte, A. M. & Peltier, W. R., 1987. Plate tectonics and aspherical Earth structure: the importance of poloidal-toroidal coupling, *J. geophys. Res.*, **89,** 3645–3679.

Froidevaux, C., 1973. Energy dissipation and geometric structure at spreading plate boundaries, *Earth planet. Sci. Lett.*, **20,** 419–424.

Gantmacher, F. R., 1960. *The Theory of Matrices*, translated by K. A. Hirsh, Chelsea Publishing, New York.

Gasperini, P., Yuen, D. A. & Sabadini, R., 1992. Postglacial rebound with a non-Newtonian upper mantle and a Newtonian lower mantle rheology, *Geophys. Res. Lett.*, submitted.

Hager, B. H., Clayton, R. W., Richards, M. A., Comer, R. P. & Dziewonski, A. M., 1985. Lower mantle heterogeneity, dynamic topography and the geoid, *Nature*, **313,** 541–545.

Hager, B. H. & Clayton, R. W., 1989. Constraints on the structure of mantle convection using seismic observations, flow models and the geoid, in *Mantle Convection, Plate Tectonics and Global Dynamics*, pp 657–763, ed. Peltier, W. R., Gordon & Breach Scientific Publishers.

Hager, B. H. & O'Connell, R. J., 1978. Subduction zones dip angles and flow driven in the Earth's mantle, *Tectonophysics*, **50,** 111–133.

Hager, B. H. & O'Connell, R. J., 1979. Kinematic models of large scale flow in the Earth's mantle, *J. geophys. Res.*, **84,** 1031–1048.

Jones, M. N., 1985. *Spherical Harmonics and Tensors for Classical Field Theory*, Research Studies Press Ltd., Letchword.

Karato, S., 1988. The role of recrystallization in the preferred orientation of olivine, *Phys. Earth. planet. Interiors*, **51,** 107–122.

Malevsky, A. V. & Yuen, D. A., 1991. Strongly chaotic non-Newtonian mantle convection, *Geophys. Astrophys. Fluid Dynamics*, in press.

Montagner, J.-P. & Tanimoto, T., 1991. Global upper-mantle tomography of seismic velocities and anisotropies, *J. geophys. Res.*, **96,** 20337–20352.

Nataf, H.-C., Nakanishi, I. & Anderson, D. L., 1986. Measurements of mantle wave velocities and inversion for lateral heterogeneities and anisotropy, 3. Inversion. *J. geophys. Res.*, **91,** 7261–7307.

Nečas, J. & Hlaváček, I., 1981. *Mathematical Theory of Elastic and Elastico-Plastic Bodies: An Introduction*, Elsevier, Amsterdam.

O'Connell, R. J. & Hager, B. H., 1991. Toroidal-poloidal partitioning of lighospheric plate motions, in *Glacial Isostasy, Sea-Level and Mantle Rheology*, pp. 535–552, eds, Sabadini R. *et al.*, Kluwer Academic Publishers, Netherlands.

Olson, P. & Bercovici, D., 1991. On the equipartition of kinetic energy in plate tectonics, *Geophys. Res. Lett.*, **18,** 1751–1754.

Parmentier, E. M., Turcotte, D. L. & Torrance, K. E., 1976. Studies of finite amplitude non-Newtonian thermal convection with application to convection in the Earth's mantle, *J. geophys. Res.*, **81,** 1839–1846.

Phinney, R. A. & Burridge, R., 1973. Representation of the elastic-gravitational excitation of a spherical Earth model by generalized spherical harmonics, *Geophys. J. R. astr. Soc.*, **74,** 451–487.

Poirier, J. P., Peyronneau, J., Gesland, J. Y. & Brebec, G., 1983. Viscosity and conductivity of the lower mantle: an experimental study on a M_gSiO_3 perovskite analogue, $KZnF_3$, *Phys. Earth. planet. Interiors*, **32,** 273–287.

Ranalli, G., 1991. The microphysical approach to mantle rheology, in *Glacial Isostasy, Sea-Level and Mantle Rheology*, pp. 343–378, eds, Sabadini R. *et al.*, Kluwer Academic Publishers, Netherlands.

Ribe, N. M., 1992. The dynamics of twin shells with variable viscosity and the origin of toroidal flow, *Geophys. J. Int.*, **110,** 537–552.

Ricard, Y. & Bai Wuming, 1991. Inferring the viscosity and the 3-D density structure of the mantle from geoid, topography and plate velocities, *Geophys. J. Int.*, **105,** 561–571.

Ricard, Y., Fleitout, L. & Froidevaux, C., 1984. Geod heights and lithospheric stresses for a dynamic Earth. *Ann. Geophysicae*, **2,** 267–286.

Ricard, Y. & Vigny, C., 1989. Mantle dynamics with induced plate tectonics, *J. geophys. Res.*, **94,** 17543–17559.

Ricard, Y., Vigny, C. & Froidevaux, C., 1989. Mantle heterogeneities, geoid and plate motions: a Monte-Carlo inversion, *J. geophys. Res.*, **94,** 13739–13754.

Ricard, Y., Froidevaux, C. & Fleitout, L., 1988. Global plate motion and the geoid: a physical model, *Geophys. J. R. astr. Soc.*, **93,** 477–484.

Richards, M. A. & Hager, B. H., 1984. Geoid anomalies in a dynamic Earth, *J. geophys. Res.*, **89,** 5987–6002.

Richards, M. A. & Hager, B. H., 1989. Effects of lateral viscosity variations on long-wavelength geoid anomalies and topography, *J. Geophys., Res.*, **94,** 10 299–10 313.

Stewart, C. A., 1992. Thermal convection in the Earth's mantle: mode coupling induced by temperature-dependent viscosity in a three dimensional spherical shell, *Geophys. Res. Lett.*, **19,** 337–340.

Van Den Berg, A. P., Yuen, D. & Van Keken, P. E., 1992. Effects of depth-variation in creep laws on the formation of plates in mantle dynamics. *Geophys. Res. Lett.*, in press.

Woodhouse, J. H. & Dziewonski, A. M., 1984. Mapping the upper mantle: Three dimensional modeling of Earth structure by inversion of seismic waveforms, *J. Geophys. Res.*, **89,** 5953–5986.

Wu P., Deformation of an incompressible viscoelastic flat Earth with power law creep: a finite element approach, *Geophys. J. Int.*, **108,** 35–51.

Zhang, S. & Christensen, U., 1991. Mode coupling through laterally variable viscosity in spherical shell circulation driven by internal loads, *Ann. Geophysicae* (Supplement) **9,** 65.